The Dispersion Solution for the New COS/FUV Cenwave G160M/1533

Andrew J. Fox[1], Bethan L. James[1], Elaine M. Frazer[1], Rachel Plesha[1], and Thomas Ake[1,2]

[1] Space Telescope Science Institute, Baltimore, MD
[2] Latitude, Inc.

9 April 2019

ABSTRACT

We describe the derivation of the dispersion solution for the new COS/FUV central wavelength (cenwave) setting G160M/1533. Observations of the emission-line star Epsilon Eridani were taken in 2018 June with the 1533 cenwave. The wavelength solution was derived by cross-correlating the spectrum with a high-quality calibrated STIS E140M spectrum of the target in a set of 76 wavelength windows, each containing a narrow emission line, and fitting a linear solution to minimize the pixel offsets as a function of wavelength. We derived the zeropoint and dispersion coefficients separately for the FUVA and FUVB detector segments, and added them to the DISPTAB reference file for Lifetime Position 4. This file was delivered to the reference file database in 2018 November for use by the CalCOS pipeline. The r.m.s. accuracy of the wavelength scale is 1.2 pixels (2.4 km s^{-1}) on FUVB and 2.1 pixels (4.2 km s^{-1}) on FUVA, similar to the values derived for other G160M cenwaves, and well within the target accuracy of three pixels.

Contents

1. Introduction

For Cycle 26 two new central wavelength (cenwave) settings were introduced for the COS FUV detector, G140L/800 and G160M/1533. The 1533 cenwave extends coverage at the short-wavelength end of G160M by 44 Å to overlap with the longest wavelengths covered by cenwave G130M/1222. This allows a broad range of FUV wavelengths to be covered by just two medium-resolution settings (1222 and 1533) without placing Lyα on the detector, avoiding a key contributor to gain sag. Furthermore, it allows the spectra to be observed at high S/N, since (unlike 1291) all four FP-POS positions can be used with both 1222 and 1533, and then coadded to mitigate fixed-pattern noise.

This report forms one of a number of ISRs on the calibration of the new 1533 cenwave. We describe the derivation of the wavelength solution, which is encoded in the DISPTAB reference file used by the CalCOS pipeline. This ISR is a partner to the ISRs on the focusing of the 1533 cenwave (James et al. 2019a), the creation of the lamp template (LAMPTAB; James et al. 2019b), the spectral extraction algorithm (XTRACTAB, TWOZXTAB, PROFTAB, TRACETAB; Frazer et al. 2019), and the flux calibration (FLUXTAB, Fox et al. 2019). Together these reference files were delivered to the Calibration Reference Database System (CRDS) on 2018 November 20, updated for both 1533 and 800, for use with Cycle 26 observations.

In this ISR we assume that the dispersion solution for 1533 is a linear polynomial, such that the wavelength λ in Å is related to the pixel number according to

$$\lambda = a_0 + a_1 x, \tag{1}$$

where a_0 is the zeropoint in Å, a_1 is the dispersion in Å pixel^{-1}, and x is the XFULL pixel number. This linear function of x differs from the G140L/800 wavelength solution, which uses a quadratic function (Fischer et al. 2019). Linear solutions have been shown to be an accurate description of the wavelength scale for the other G160M cenwaves at all lifetime positions (LPs; Plesha et al. 2018, 2019a,b for LP1, LP3, and LP4; Ake et al. 2019 for LP2), and we show in this ISR that linearity is also a good assumption for the 1533 cenwave.[1]

---

[1] The earlier ISRs use the notation a_0 for the zeropoint and a_1 for the dispersion.

2. Observations

The emission-line star Epsilon Eridani (ϵ Eri) was observed in the G160M/1533 setting on 2018 June 24 in a one-orbit observation under Program 15457, "COS/FUV/G160M/1533 Wavelength Calibration - Dispersion Solution" (PI A. Fox). ϵ Eri is a bright K dwarf (spectral type K2V, V magnitude = 3.73) that has been routinely used for wavelength-calibration observations for other COS FUV cenwaves at multiple lifetime positions (Plesha et al. 2019a,b). Due to its bright NUV magnitude, the acquisition images were taken with the bright object aperture (BOA) and MIRRORB. Two ACQ/IMAGE exposures were taken to optimize the centering.

Because the 1533 cenwave was not implemented in the APT proposal planning software at the time the observations executed, the observation was commanded in a non-standard manner. First, we configured G160M/1577 (the nearest cenwave to 1533) using a dummy 0.1 s exposure, and then we used an "ALIGN OSM" exposure to set the focus mechanism to the 1533 focus and rotation position. The 1577-to-1533 focus offset of -538 was derived from the focus sweep program (James et al. 2019a), and the 1577-to-1533 rotation offset was +15 according to ray-trace optical models (S. Penton, private communication). We then executed a single science exposure with 1533 with FP-POS = 3 and an exposure time of 1952 s (dataset `ldsh01jhq`). FP-POS = 3 was chosen since this is the nominal position used to define the dispersion solution of a given cenwave. The exposure time was calculated following Program 15365, "COS FUV Dispersion Solutions at LP4" (PI R. Plesha), and ensures sufficient counts in emission lines on segments FUVA and FUVB. Specifically, a $\approx$ 2000 s exposure ensures $\approx$ 30 counts in the emission line at 1681.4 Å, ensuring a good cross-correlation with the STIS spectrum (Plesha et al. 2019a). We used special commanding to switch off calibration and disassociate the 1533 exposure, since the back-end software was (at the time of execution) not ready for processing 1533 files.

3. Data Reduction

The ϵ Eri raw data (`rawtag`) files were manually processed through CalCOS (v3.3.4) using a preliminary DISPTAB reference file that contained predicted values of the 1533 zeropoint (a_0) and dispersion (a_1). These predicted values were calculated from the values of a_0 and a_1 for the other G160M cenwaves at LP4, namely 1577, 1589, 1600, 1611, and 1623, which were contained in the first and second elements of the `coeff` array, respectively, in the LP4 DISPTAB named `249151961_disp.fits`. We extrapolated the values linearly down to 1533 (see Figure 1).

The data reduction was performed with a BOXCAR extraction using the newly derived 1533 XTRACTAB (Frazer et al. 2019) and LAMPTAB (James et al. 2019b), and using a preliminary FLUXTAB that was replicated from the 1577 FLUXTAB. (Accurate flux calibration is not necessary for the wavelength-solution analysis, and, in any case, the final 1533 FLUXTAB was unavailable since it was derived later in the reference-
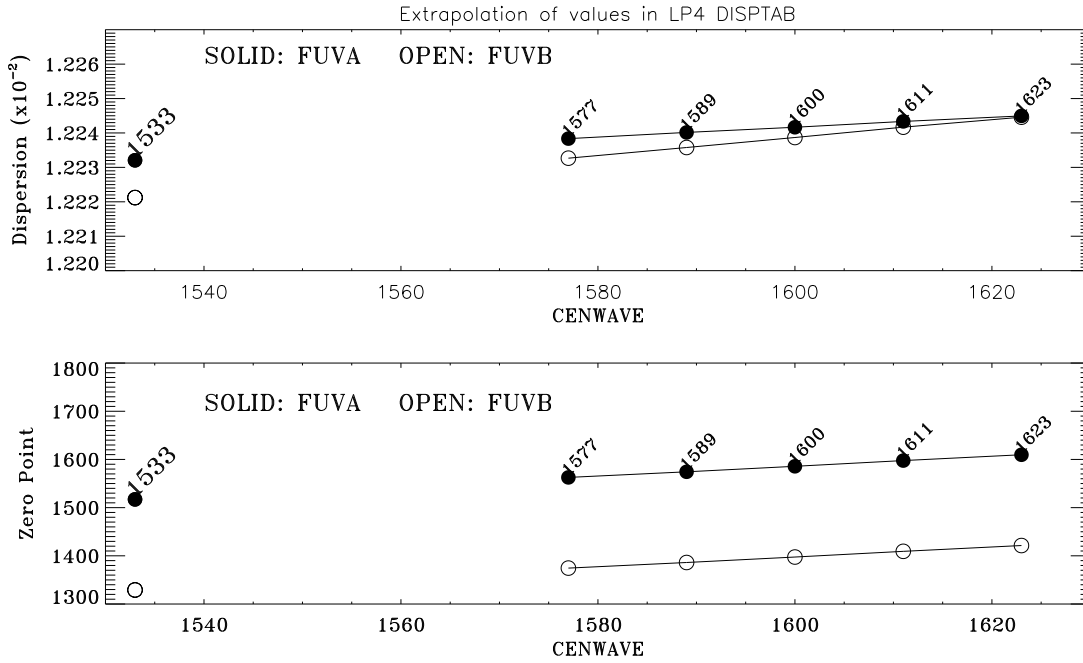
Figure 1. Extrapolation of the dispersions (top panel, in units of 10^{-2} Å pixel^{-1}) and zeropoints (lower panel, in Å) from the five other G160M cenwaves down to 1533, using the values from the LP4 DISPTAB. These extrapolations were used to calculate the *preliminary* values of Z and D in the 1533 DISPTAB.

file creation process; Fox et al. 2019). A TWOZONE extraction was not possible since the TWOZXTAB, PROFTAB, and TRACETAB references file were also created later in the process (Frazer et al. 2019), hence the choice of the BOXCAR extraction. The reduction resulted in a single extracted spectrum (`xld` file). A summary of the CalCOS calibration switches used in the reduction is given in Table 1.

4. Derivation of the Dispersion Solution

The extracted 1-D spectrum of ϵ Eri was analyzed using a custom-developed IDL routine that uses cross-correlation techniques to compare the 1533 spectrum to a high-S/N STIS E140M spectrum of the target. This STIS spectrum is treated as error-free, since the STIS echelle modes can be wavelength-calibrated to high accuracy (0.2–0.3 pixels; Welty et al. 2018). The comparison is conducted in a series of 76 windows, 42 on detector segment FUVA and 34 on FUVB, following the same windows used to calibrate the other G160M cenwaves (Plesha et al. 2019a). Each window contains a narrow emission line and is vetted to ensure there is no evidence for variability. We determined the COSxSTIS cross correlation function (CCF) in each of these 76 windows, using

Table 1. Calibration Switches Used to Process Raw Program 15457 Data in CalCOS[1]

Calibration Step	Value	Description
FLATCORR	PERFORM	Apply flat-field correction
DEADCORR	PERFORM	Correct for deadtime
DQICORR	PERFORM	Data quality initialization
TEMPCORR	PERFORM	Correct for thermal distortion
GEOCORR	PERFORM	Correct FUV for geometic distortion
DGEOCORR	PERFORM	Delta Corrections to FUV Geometric Distortion
IGEOCORR	PERFORM	Interpolate geometric distortion in INL file
RANDCORR	PERFORM	Add pseudo-random numbers to raw x and y
XWLKCORR	OMIT	Correct FUV for Walk Distortion in X
YWLKCORR	PERFORM	Correct FUV for Walk Distortion in Y
PHACORR	PERFORM	Filter by pulse-height
TRCECORR	**OMIT**	**Trace correction**
ALGNCORR	**OMIT**	**Align data to profile**
XTRCTALG	**BOXCAR**	**BOXCAR or TWOZONE**
BADTCORR	OMIT	Filter by time (excluding bad time intervals)
DOPCORR	PERFORM	Orbital Doppler correction
HELCORR	PERFORM	Heliocentric Doppler correction
X1DCORR	PERFORM	1-D spectral extraction
BACKCORR	PERFORM	Subtract background (when doing 1-D extraction)
WAVECORR	PERFORM	Use wavecal to adjust wavelength zeropoint
FLUXCORR	PERFORM	Convert count-rate to absolute flux units
BRSTCORR	**OMIT**	**Switch controlling search for FUV bursts**
TDSCORR	PERFORM	Switch for time-dependent sensitivity correction

[1]Calibration steps shown in gray are defaults, whereas those in black have been changed from the default.

the IDL `c_correlate` function,[2] then fit a Gaussian function to the CCF in each window to determine the lag, which represents the offset in pixels between the COS and STIS wavelength solutions. For this analysis we did not rebin or convolve the STIS E140M spectrum before cross-correlation, because we wanted to preserve maximum resolution information, but we did resample it to the COS wavelength grid using linear interpolation. We used heliocentric wavelengths throughout the analysis (for both COS and STIS spectra) to ensure all wavelengths were referenced to the same system. The heliocentric correction for the ϵ Eri dataset was –18.1 km s^{-1}. The cross-correlation technique is illustrated in Figure 2.

By plotting the pixel offset (lag) against heliocentric wavelength, any slope and/or zeropoint offset in the wavelength solution becomes evident. This technique is illustrated in the top panel of Figure 3 for each detector segment, where a clear slope is seen on both FUVA and FUVB. We conducted linear fits to the pixel offsets on each segment, finding the slopes s and intercepts C annotated on the plot. We calculated updated values of the dispersion a_1 and zeropoint a_0 by removing the slope and intercept on each segment, according to

$$a_1^{\text{updated}} = a_1^{\text{prelim}}(1 + sa_1^{\text{prelim}})$$
$$a_0^{\text{updated}} = a_0^{\text{prelim}} + \delta a_0^{\text{coarse}} + \delta a_0^{\text{fine}} = a_0^{\text{prelim}} + \delta a_0^{\text{coarse}} + Ca_1^{\text{prelim}}, \qquad (2)$$

where a_0^{updated} and a_1^{updated} are calculated separately on each detector segment. Note there are two corrections to the zeropoint: a coarse correction $\delta a_0^{\text{coarse}}$ determined from the global (full-spectrum) COS-STIS cross-correlation to bring the offsets close to zero, and a fine correction $\delta a_0^{\text{fine}} = Ca_1^{prelim}$ determined from the line-by-line cross-correlation (i.e., from the y-intercept of the top panel of Figure 3). In principle the two corrections could be combined into one, but we found it expedient to break them into two. Note that a_1^{prelim} appears in the final term of each equation, since the two axes on Figure 3 have different units: the y-axis is in pixels and the x-axis in Angstroms. The inclusion of a_1^{prelim} in these terms ensures the corrections to a_0 and a_1 have the right units. The preliminary and updated values determined in this manner are given in Table 2.

We then created a new DISPTAB reference file replacing the preliminary values with the updated values, then reprocessed the raw data through CalCOS a second time, using the new DISPTAB. When we re-ran the auto-correlation analysis and recreated the plot of offset versus wavelength, we verified that the slope and zeropoint offset had been removed (see lower panel of Figure 3). The values of the dispersion and zeropoint derived and implemented in the updated DISPTAB are summarized for all apertures in Table 3. Note that we set the WCA/1533 dispersion equal to the WCA/1577 dispersion and the WCA/1533 zeropoint equal to the PSA/1533 zeropoint to account for the different optical path through the WCA, but these values have not been tested and

---

[2]We also explored the effects of instead using the IDL `cross_correlate` function or the Python `correlate` function and found minor but insubstantial differences in the results.
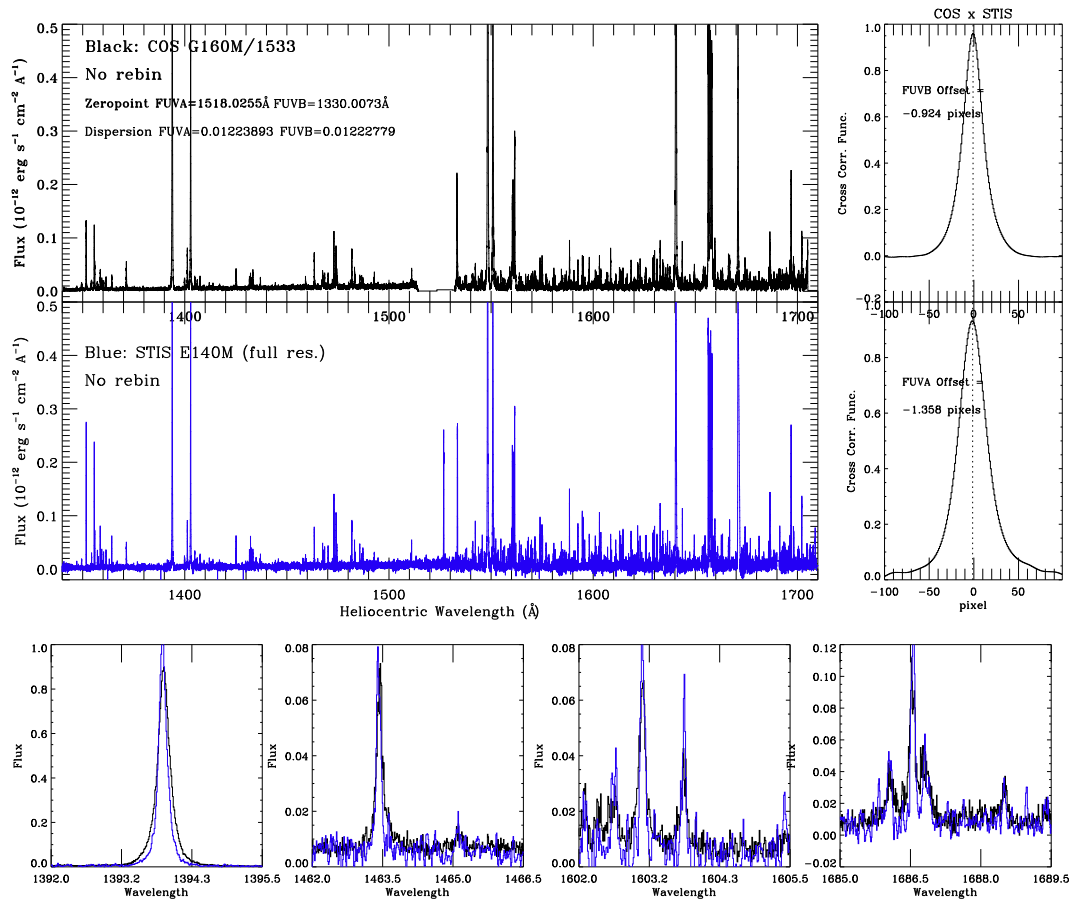
Figure 2. Illustration of the cross-correlation technique used to derive the 1533 dispersion solution from observations of ϵ Eri. The top-left panel shows the COS 1533 observations calibrated using the preliminary dispersion (black). The middle-left panel shows the STIS E140M spectrum (blue) used as the reference spectrum. The top-right (FUVB) and middle-right (FUVA) panels show the global COS-STIS cross-correlation functions (CCFs), which quantify how well the COS and STIS spectra are aligned. Gaussian fits to the CCFs are used to identify the offsets. The bottom panels show zoomed-in regions around four of the emission lines used for the cross-correlation. In our analysis, we measure the CCF around 74 individual emission lines and plot the offsets against wavelength (see Figure 3).

should not be used in practice. The r.m.s. accuracy of the wavelength scale (as measured by the dispersion in the pixel offsets) is 1.2 pixels (2.4 km s^{-1}) on FUVB and 2.1 pixels (4.2 km s^{-1}) on FUVA. The larger scatter on FUVA is a known phenomenon, which is seen at similar magnitude for the other G160M wavelengths (Plesha et al. 2019b), and is due to the larger geometric distortion on FUVA. These values are well within the target COS wavelength solution accuracy of 3 pixels (7.5 km s^{-1}) and certainly within the advertised accuracy of of 15 km s^{-1} (COS Instrument Handbook).

Figure 3. *Top:* Plot of offset in pixels (in the sense COS − STIS) versus heliocentric wavelength, using the *preliminary* dispersion solution. Each data point represents a different emission line. A clear slope in the offsets is visible on both detector segments. We conducted linear fits to the offsets on each segment (see legend) and used these to adjust the dispersion to remove the slope and refine the zeropoint using Equation 2. *Bottom:* Same as top panel, except now using the *updated* dispersion solution. The slope and zeropoint offset have been removed on each detector segment. The mean and standard deviation of the offsets are annotated on the plot. Note how the standard deviation of the residuals is larger by a factor of ≈ 2 on FUVA than on FUVB.

Table 2. Preliminary and Updated Dispersion Coefficients for G160M/1533[1]

| Segment	a_1^{prelim} (Å pixel^{-1})	a_1^{final} (Å pixel^{-1})	a_0^{prelim} (Å)	a_0^{final} (Å)
FUVA	0.01223206	0.01223893	1517.0957	1518.0255
FUVB	0.01222123	0.01222779	1329.1478	1330.0073

[1]All values in this table are derived for the PSA. See Table 3 for other apertures.

Table 3. Summary of Dispersion Solution Coefficients for 1533

Aperture	Segment	Dispersion a_1 (Å pixel^{-1})	Zeropoint a_0 (Å)
PSA	FUVA	0.01223893	1518.0255
PSA	FUVB	0.01222779	1330.0073
BOA[1]	FUVA	0.01223893	1518.0255
BOA[1]	FUVB	0.01222779	1330.0073
WCA[2]	FUVA	0.01224400	1518.0255
WCA[2]	FUVB	0.01223800	1330.0073

[1]BOA values of a_1 and a_0 are set equal to the corresponding PSA values.

[2]WCA dispersion is set to 1577 dispersion; WCA zeropoint is set to PSA zeropoint.
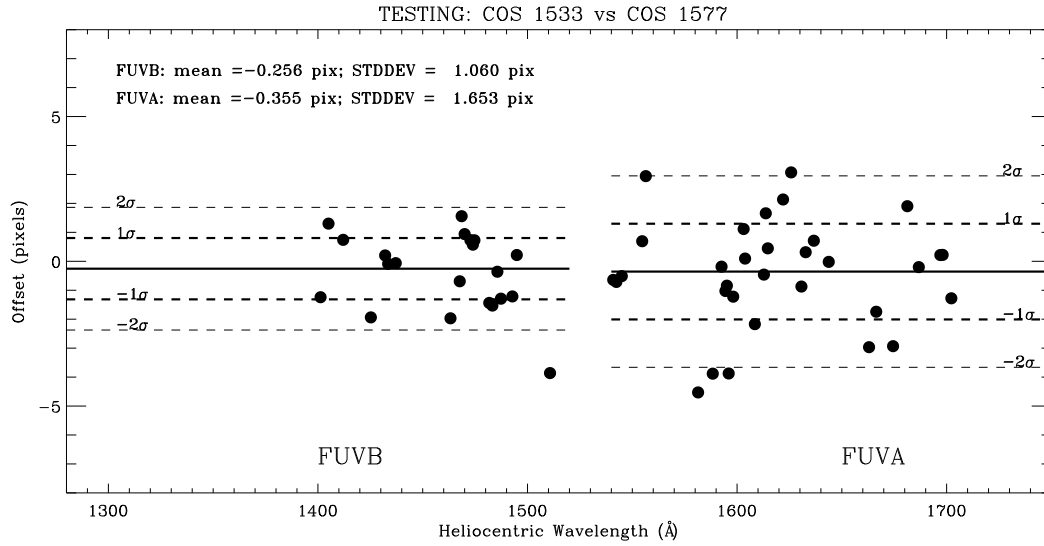
Figure 4. Testing of the newly created 1533 DISPTAB. This plot has the same format as Figure 3, showing pixel offsets versus wavelength, but now we are comparing to existing calibrated COS/FUV G160M/1577 data of ϵ Eri rather than to the STIS spectrum. The lack of a significant zeropoint offset or slope on either segment confirms the validity of the dispersion solution.

5. Testing the DISPTAB

We tested the new 1533 DISPTAB in two separate ways. First, we compared the resulting wavelength solution in the reprocessed data of ϵ Eri to an existing calibrated COS FUV dataset of the same target taken at LP4 with the G160M/1577 cenwave. For this comparison, we chose 1577 dataset `ldnq03020`, taken on 2017 August 14 under Program 15365 (PI R. Plesha), the LP4 wavelength calibration program. We compared the pixel offsets from a cross-correlation analysis in exactly the same way as in Figure 3, except now using a COS vs. COS comparison (1533 vs. 1577) instead of a COS vs. STIS comparison. The results are shown in Figure 4. Notice how there are no points below 1400 Å, because this test only works for wavelength ranges covered by both 1533 and 1577. We find no slope or significant zeropoint offset on either segment, indicating the 1533 dispersion solution is consistent with the 1577 dispersion solution, so this test of the 1533 DISPTAB can be considered successful. We also notice a larger dispersion on FUVA than FUVB, as expected.

The second check of the validity of the dispersion solution is to compare the derived dispersion to expectations from the focus-dispersion relation, which has been shown to hold for other G160M cenwaves (Ake et al. 2019). The relations for all lifetime positions are shown in Figure 5 (updated from Plesha et al. 2019b). For detector segment FUVB, the derived dispersion (12.2278±0.0006 mÅ pixel^{-1}) exactly matches the linearly extrapolated value (12.228 mÅ pixel^{-1}) from the LP4
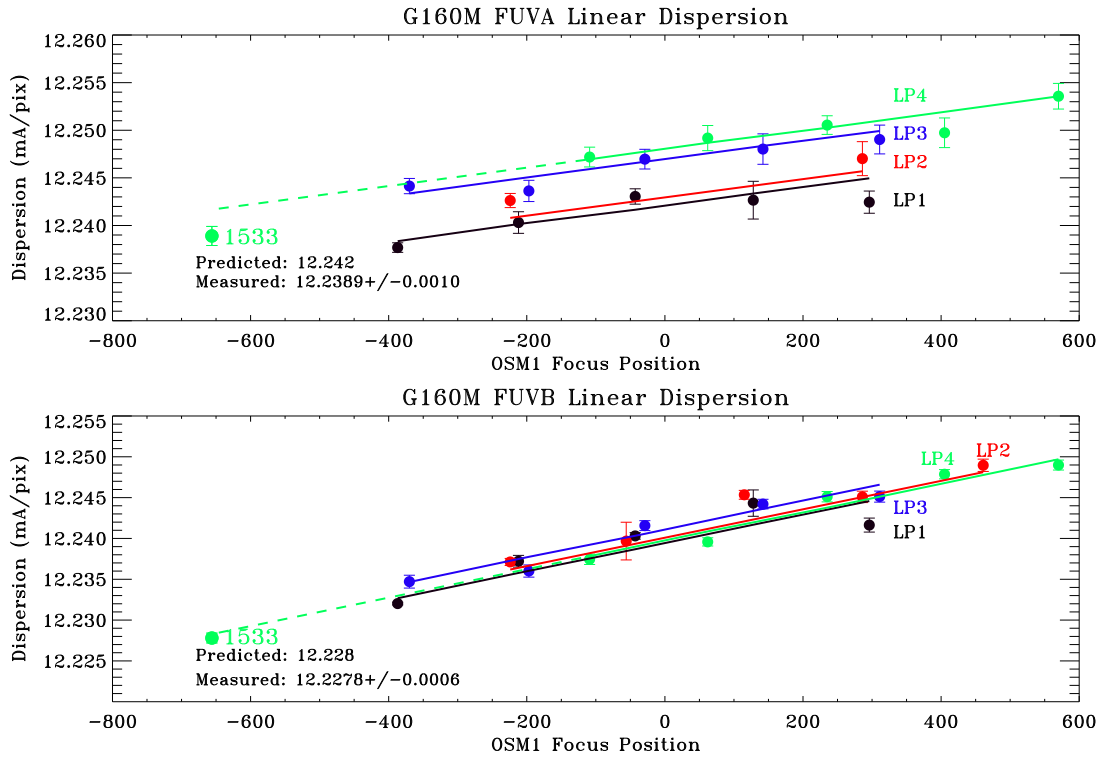
Figure 5. Focus-dispersion relation for COS/FUV G160M cenwaves for segment FUVA (top) and FUVB (bottom), updated from Plesha et al. (2019b). Data from several lifetime positions (LPs) are shown in different colors, as indicated on the plot. The 1533 cenwave is at focus position -646, several hundred focus steps away from the other settings. The predicted (extrapolated) and derived (from this analysis) dispersions for 1533 are annotated on the plots, in units of mÅ pixel^{-1}. Note how the error bars are smaller on FUVB than on FUVA for all LPs, a result of the smaller geometric distortion on that segment. Dashed lines are linear extrapolations from the 1577 to 1623 cenwaves at LP4.

focus-dispersion relation for cenwaves 1577 through 1623. However, for FUVA, we find the derived dispersion (12.2389±0.0010 mÅ pixel^{-1}) is $\approx 3\sigma$ *below* the predicted value (12.242 mÅ pixel^{-1}). The offset indicates that the G160M focus-dispersion relation for FUVA cannot be linearly extrapolated from the other cenwaves over large focus intervals to shorter wavelengths. (There are 538 rotation motor steps between 1577 and 1533, a significant interval.) This is not surprising, since the alignment of the focus-dispersion relations for each lifetime position is not as tight for FUVA as for FUVB (see Figure 5), indicating FUVA has a more complex relation of dispersion with focus.

6. Summary

The G160M/1533 dispersion and zeropoints for each aperture (PSA, BOA, and WCA) and both segments (FUVA and FUVB) derived in this analysis were merged into the DISPTAB submitted to the CRDS reference-file database on 2018 November 20. The new DISPTAB (named `2bj2256ml_disp.fits`) contains entries for both cenwaves 1533 and 800 and is in use for LP4 observations from Cycle 26 onward. The r.m.s. accuracy of the 1533 wavelength scale is 1.2 pixels (2.4 km s^{-1}) on FUVB and 2.1 pixels (4.2 km s^{-1}) on FUVA, well within the nominal COS wavelength solution accuracy of 3 pixels, and similar to the performance of the other G160M cenwaves.

Change History for COS ISR 2019-10

Version 1: 9 April 2019 – Original Document

References

Ake, T., Plesha, R., De Rosa, G., et al. 2019, COS ISR 2018-23, "Improvements to the COS FUV G130M and G160M Wavelength Solutions at Lifetime Position 2"

Fischer, W., Magness, C. R., Sankrit, R., & Oliveira, C. 2019, COS ISR 2019-05, "The Dispersion Solution for the New COS/FUV Cenwave G140L/800"

Fox, A. J., James, B. L., Frazer, E. M., & Fischer, W. J. 2019, COS ISR 2019-09, "The Flux Calibration of the New COS/FUV Cenwave G160M/1533"

Frazer, E. M., Fox, A. J., James, B. L., Roman-Duval, J., & Sankrit, R. 2019, COS ISR 2019-08, "Spectral Extraction of the New COS/FUV G160M/1533 Mode: Extraction, Trace, and Profile Reference Files"

James, B., et al. 2019a, COS ISR 2019-06, "Focusing the New COS/FUV Cenwave G160M/1533"

James, B., et al. 2019b, COS ISR 2019-07, "The Lamp Template for the New COS/FUV Cenwave G160M/1533"

Plesha, R., Ake, T., De Rosa, G., Oliveira, C., & Penton, S. 2019a, COS ISR 2018-24, "Improvements to the COS FUV G130M and G160M Wavelength Solutions at Lifetime Position 3"

Plesha, R., Ake, T., De Rosa, G., Oliveira, C., & Penton, S. 2019b, COS ISR 2018-25, "Improvements to the COS FUV G130M and G160M Wavelength Solutions at Lifetime Position 4"

Plesha, R., Ake, T., De Rosa, G., et al. 2018, COS ISR 2018-22, "Improvements to the COS FUV G130M and G160M Wavelength Solutions at Lifetime Position 1"

Welty, D. 2018, STIS ISR 2018-04, "Monitoring the STIS Wavelength Calibration: MAMA and CCD First-Order Modes"